International Journal of Scientific Research and Engineering Development-– Volume 3 - Issue 5, Sep - Oct 2020

Available at www.ijsred.com

RESEARCH ARTICLE OPEN ACCESS

Rayleigh Model of Radiation Heat Transfer in Spherical Medium

Hamza Mohamed*
University of Dayton
300 College Park Drive
Dayton, Ohio, USA
Mohamedh1@udayton.edu

ABSTRACT

In certain extremely low probability, severe accident scenarios which have been postulated for liquid metal cooled fast reactors, large bubble cavities containing fuel vapor and fission products transit a layer of coolant and release this material to the cover gas thereby presenting a contribution to an accident-specific source term [5]. Rayleigh model in radiation heat transfer has been investigated to analysis and interpret the experiments that conducted during 1980's for oxide UO_2 fueled reactors in Fuel Aerosol Simulant Test (FAST) facility at Oak Ridge National Laboratory (ORNL).These analyses are applied to estimate the bubble collapse of Liquid Metal reactors (LMR's) during a hypothetical core disruptive accident (HCDA). In Rayleigh non-scattering model the particle size was 0.01 µm [6],and according to Mie theory principle, the absorption coefficient for small particle –size distribution was estimated (k = 10 m^{-1} was used) from reference [7] at complex refractive index of UO_2 at λ = 600 µm and x = 0.0785.A MATLAB code was used to solvethe radiative heat equation (RTE) in spherical coordinates. The mixture is in local thermodynamic equilibrium inside the bubble which has a black body surface boundary.The mixture in the cavity contains three components: the non-condensable gas Xenon, Uranium dioxide vapor, and fog.To simulate fuel bubble's geometry as realistically as possible, according to experimental observation, the energy equation in a spherical coordinate system has been solved with the radiative flux heat transfer equation (RTE) to obtain the effect of fuel bubble's geometry on the transient radiative heat flux and to predict the transient temperature distribution in the participating medium during a hypothetical core disruptive accident (HCDA) for liquid metal fast breeding reactor (LMFBR) for FAST. The transient temperature distribution in fog region was utilized to predict the amount of condensable UO_2 vapor $m_{fog} = \frac{4\pi C_0 M_{UO_2}}{k^3} \int_{\tau_f}^{\tau_o} [x_{sat} - g_0(T)]\tau^2 d\tau$. The conclusion that can be drawn from the present study, is that the Fuel Aerosol Simulant Test (FAST) facility at Oak Ridge National Laboratory has a larger margin of safety since the bubble rising time is greater than the bubble collapse time.

KEYWORDS
Rayleigh, accidents, radiation,extreme events.

1. INTRODUCTION

The hypothetical core disruptive accident (HCDA) will occur when there is no coolant flow inside the cooling channels among the fuel rods. Conditions such as this may include for example the failure of circulation pumps, control room systems, and control rods.When the reactor is at full load, and the cooling system is in a failure state, the fuel in the core starts to heat up or boil and the vapor can leave the reactor as shown in Figure 1 [8].As the fuel starts vaporizing, UO_2 vapor and non-condensable Xe gas are produced from the fission chain reaction. The bubbles expand radially and axially at high temperature and pressure, leaving the core and proceeding to

the coolant pool as it is indicated in Figure 1[8]. The mechanism of this transfer could occur due to multiphase bubbles which contain "fuel vapor, fission gas, and UO_2 particles" [9]. LMR's are becoming an increasingly important in the field of nuclear engineering. More efforts should be encouraged to study, analyze, and to improve the performance of fast neutron reactors. Safety issues should especially be addressed so that possible negative impacts can be mitigated.

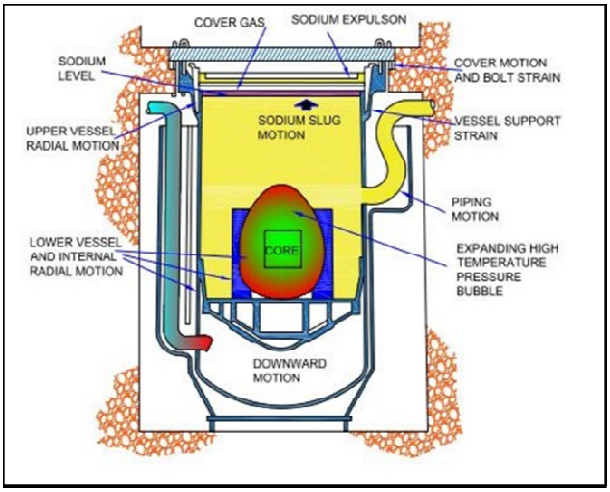

Figure 1. Reactor geometry (adapted from WTT) [74].

In the past, a safety analysis of a liquid metal fast breeder reactor (LMFBR) was studied by Michael et al. (1979) using an experimental model describing two-phase liquid flow motion with coolant vaporization phenomena and without external thermal radiation effects.Kress et al. (1977) presented a significant examination of nuclear reactor safety research regarding the study of important parameters affecting two phase flow generated during a hypothetical core disruptive accident (HCDA).Tobias et al. (1979) was to study the heat and mass transfer arising from a Uranium dioxide (UO_2) bubble for the sodium experiment in the Fuel Aerosol Simulant Test (FAST) facility. A. B. Reynolds et al. (1979) illustrated bubble behavior experiments.The expansion of two phase UO_2 in a tank of inviscid and incompressible coolant has been analyzed by A. B. Reynolds et al. (1987) using the UVABUBL computer model.H. Chan et al. (1979) investigated the condensation phenomena and heat transfer from a very hot mixture of gases at 4050 K to a low temperature field boundary consisting of a sodium coolant at 823 K. R. L. Webb et al. (1985) have analyzed the heat and mass transfers at ORNL for UO_2 bubble under sodium FAST tests by using the UVABUBL II Package.Recent studies [1-5] regarding hypothetical, severe accident events in sodium-cooled as well as lead-cooled configurations have considered the impact on accident progression of the formation and presence of vapor bubble cavities within the coolant, where the cavities may contain various mixtures of fission products, combined in some cases with fuel, coolant and structural materials [10].

The objective of the present study is to study the effect of the fuel bubble's geometry on radiative heat flux and transient temperature distribution in a participating medium during a hypothetical core disruptive accident (HCDA) for liquid metal cooled reactor (LMR), and to study the vapor bubble behavior, in particular the bubble collapse is of interest. for a stationary, spherical bubble containing fuel vapor (UO_2), fission gas (Xe) at high temperature (4050 K) surrounded by Sodium coolant (811 K) [9, 10].

2. RADIATION ANALYSIS

The system as described is under local thermodynamic equilibrium, and radiation dominates the heat transfer. Furthermore, the thermodynamic properties of UO_2 vapor and Xe gas are assumed constant, and the vapor and gas are modelled as a perfect gas [12, 13]. Under these conditions, it was also assumed that the effects of other types of heat and mass transfer can be neglected such as convection, conduction and diffusion as compared with the radiation heat transfer where it is radiating at high temperatures as shown in (Fig. 2) [13].Mie theory will be employed to ascertain the amount of radiative energy that is lost due to the presence of UO_2 particles within the medium in the model. The magnitude of the energy reduction can be determined by computing the absorbing coefficient of the participating medium [14, 11].

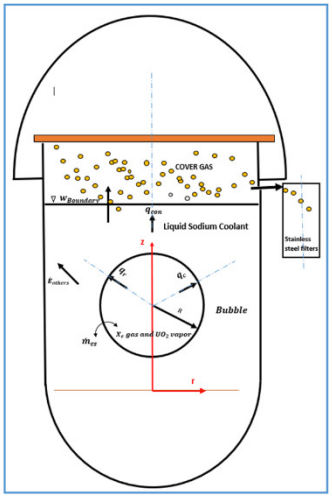

Figure 2. Configuration of bubble and LMR reactor.

The spherical coordinate system for the equation of radiative heat transfer (RTE) has the following form [15, 17].

$$\mu\frac{\partial I_\lambda\ (\mathrm{r},\mu)}{\partial \mathrm{r}}+\frac{1-\mu^2}{\mathrm{r}}\frac{\partial I_\lambda\ (\mathrm{r},\mu)}{\partial \mu}+\beta_\lambda I_\lambda\ \ (\mathrm{r},\mu)=\ k_\lambda I_{\lambda b}(\mathrm{T})+\tfrac{1}{2}\sigma_\lambda\int_{-1}^{1}p(\mu,\mu')I(\mathrm{r},\mu')\,\mathrm{d}\mu' \quad (1)$$

The first and the second terms of the above equation represents the change of I (r, μ) intensity with respect to r and μ directions. The third term represents the reduction of the radiation due to the absorption and out scattering effect on the thermal radiation wave that is propagating in the medium. Both terms on the right-hand side of Equation (1) represent the augmentation of I (r, μ) intensity where $I_{\lambda b}(\tau)=\frac{n^2\sigma T^4(\tau)}{\pi}$ and by neglecting the scattering effects and assuming azimuthal symmetry [30] in Equation (1) gives us:

$$\frac{\mathrm{d}I_\lambda\ (\mathrm{r},\mu)}{d\tau_\lambda}+\frac{1}{\mu}I_\lambda\ \ (\mathrm{r},\mu)=\ \frac{(1-\omega_\lambda)}{\pi\mu}e_{\lambda b}(\tau) \quad (2)$$

Where $e_{\lambda b}(\tau)$is the black – body monochromatic emissive power.β_λ andk_λ are the spectral extinction and the spectral absorption coefficients with m^{-1}. $\tau_\lambda=\int_0^r\beta_\lambda\,dr$ is the optical depth, $\mu=cos\theta$ is the direction of cosine and $\omega_\lambda=\frac{\sigma_\lambda}{\beta_\lambda}$ is the spectral albedo where σ_λ is

the spectral scattering coefficient m^{-1}[15].
The boundary conditions of Equation (2) are[17]:

$$I_\lambda^+(\tau_\lambda,\mu) = I_\lambda^+(0,\mu) \quad (3)$$

$$I_\lambda^-(\tau_\lambda,\mu) = I_\lambda^-(\tau_{0\lambda},-\mu) \quad (4)$$

Equation (2) is a non–homogenous ordinary differential equation that can be solved with Equations (3,4) by using integrating factor method or the variation of parameters method[17].

$$I_\lambda^+ = \frac{1}{\pi}\int_0^{\tau_\lambda}\left[\frac{k_\lambda}{\beta_\lambda}e_{b\lambda}(\mathrm{t})\quad e^{-\frac{(\tau_\lambda-t)}{\mu}}\frac{dt}{\mu}\right] + \quad I_\lambda^+(0,\mu)e^{\frac{-\tau_\lambda}{\mu}} \quad (5)$$

$$I_\lambda^- = \frac{-1}{\pi}\int_{\tau_\lambda}^{\tau_{0\lambda}}\left[\frac{k_\lambda}{\beta_\lambda}e_{b\lambda}(\mathrm{t})\right]\quad e^{-\frac{(\tau_\lambda-t)}{\mu}}\frac{dt}{\mu} \quad + I_\lambda^-(\tau_{0\lambda},\mu)e^{\frac{(\tau_{0\lambda}-\tau_\lambda)}{\mu}} \quad (6)$$

The monochromatic radiation flux can be calculated from the following formula [10].

$$q_R''(\lambda) = \ 2\pi\int_{-1}^{1} I_\lambda(\tau_\lambda,\mu)\mu d\mu \quad (7)$$

$$q_R''(\lambda) = \ 2\pi\int_0^1 I_\lambda^+(0,\mu)e^{\frac{-\tau_\lambda}{\mu}}\mu d\mu - 2\pi\int_0^1 I_\lambda^-(\tau_{0\lambda},-\mu)e^{\frac{-(\tau_{0\lambda}-\tau_\lambda)}{\mu}}\mu d\mu + 2\int_0^{\tau_\lambda}\frac{k_\lambda}{\beta_\lambda}e_{b\lambda}(\mathrm{t})E_2(\tau_\lambda - t)dt - 2\int_{\tau_\lambda}^{\tau_{0\lambda}}\frac{k_\lambda}{\beta_\lambda}e_{b\lambda}(\mathrm{t})E_2(t-\tau_\lambda)dt \quad (8)$$

Where $E_n(t) = \int_0^1 \mu^{n-2}e^{\frac{-t}{\mu}}d\mu$ is exponential integrals [17]andthe divergence of radiative flux becomes$\int_0^\infty q_R''(\lambda)d\lambda = \int_0^\infty \frac{1}{r^2}\frac{\partial}{\partial r}\left(r^2 q_R''(\lambda)\right)d\lambda = \int_0^\infty \frac{B_\lambda}{\frac{dq_R''(\lambda)}{d\tau_\lambda}}d\lambda + \int_0^\infty \frac{2B_\lambda}{\tau_\lambda}\ q_R''(\lambda)\ d\lambda$ (9)

$$-\frac{dq_R''(\lambda)}{d\tau_\lambda} = \ 2\pi\int_0^1 I_\lambda^+(0,\mu)e^{\frac{-\tau_\lambda}{\mu}}d\mu + 2\pi\int_0^1 I_\lambda^-(\tau_{0\lambda},-\mu)e^{\frac{-(\tau_{0\lambda}-\tau_\lambda)}{\mu}}d\mu + 2\int_0^{\tau_\lambda}\frac{k_\lambda}{\beta_\lambda}e_{b\lambda}(\mathrm{t})E_1(\tau_\lambda - t)dt + 2\int_{\tau_\lambda}^{\tau_{0\lambda}}\frac{k_\lambda}{\beta_\lambda}e_{b\lambda}(\mathrm{t})E_1(t-\tau_\lambda)dt - 4\left\{\frac{k_\lambda}{\beta_\lambda}e_{b\lambda}(\tau_\lambda)\right\} \quad (10)$$

Next, the gray medium approximation can be applied. Which says that the absorption and extinction coefficient are independent of the wavelength. This permits Equations (9, 10) to be re-written in as [15, 62]:

$$-\frac{dq_R''}{d\tau_\lambda} = \ 2\pi\int_0^1 I_\lambda^+(0,\mu)e^{\frac{-\tau}{\mu}}d\mu + 2\pi\int_0^1 I_\lambda^-(\tau_0,-\mu)e^{\frac{-(\tau_0-\tau)}{\mu}}d\mu + 2\int_0^{\tau_0}\frac{k}{\beta}\ \sigma T^4(t)E_1|\tau - t|dt - 4\frac{k}{\beta}\ \sigma T^4(t) \quad (11)$$

From reference [17], the terms for diffuse surfaces$I_\lambda^+(0,\mu)$ and$I_\lambda^-(\tau_0,-\mu)$,can be expressed in terms of surface radiosities as:

$$2\pi\int_0^1 I_\lambda^+(0,\mu)e^{\frac{-\tau_\lambda}{\mu}}d\mu = 2B_{\mathrm{w}\lambda}E_2(\tau_\lambda) \quad (12)$$

$$2\pi\int_0^1 I_\lambda^-(\tau_{0\lambda},-\mu)e^{\frac{-(\tau_{0\lambda}-\tau_\lambda)}{\mu}}d\mu = 2B_{2\lambda}E_2(\tau_{0\lambda}-\tau_\lambda) \quad (13)$$

Upon integrating Equation (11) for all wave lengths from 0→∞ Equation (11) can be written as:

$$-\frac{dq_R''}{d\tau_\lambda} = \int_0^\infty [2B_{w\lambda}E_2(\tau_\lambda) + 2B_{2\lambda}E_2(\tau_{0\lambda} - \tau_\lambda)]d\lambda + 2\int_0^\infty \int_0^\tau \frac{k}{\beta}\ \sigma T^4(t)E_1(\tau - t)dtd\lambda + 2\int_0^\infty \int_\tau^{\tau_0} \frac{k}{\beta}\ \sigma T^4(t)E_1(\tau - t)dtd\lambda - 4\int_0^\infty (1-\omega)\sigma T^4(t)\,d\lambda \quad (13)$$

If we neglect the spectral albedo of scattering, and assume that the mixture is inthermodynamic equilibrium confined between two black body surfaces boundaries, then by applying these boundary conditions, Equation (13) can be simplified, after setting [13],

$$-\frac{dq_R''}{d\tau_\lambda} = 2\sigma T_w^4 E_2(\tau) + 2\sigma T_\infty^4 E_2(\tau_0 - \tau) + 2\int_0^\tau \sigma T^4(t)\,E_1(\tau - t)dt + 2\int_\tau^{\tau_0} \sigma T^4(t)\,E_1(\tau_\lambda - t)dt - 4\sigma T^4(t) \quad (14)$$

The approximation that was used to simplify Equation (14) to Equation (15) was used in many references and gave a good result [13].

$$\frac{dq_R''}{d\tau} = 2\,E_2(\tau)\sigma T^4(\tau) \quad 0 < \tau \le \tau_o \quad (15)$$

If we neglect the spectral albedo of scattering,ω=0 =≫k= β , and assume that the mixture is in local thermodynamic equilibrium inside the bubble which has a black body surface boundary, then by applying these boundary conditions, Equation (8) can be simplified, after setting [56].

$$q_R'' = 2\sigma T_\infty^4 E_3(\tau) + 2\int_0^{\tau_o} \mathrm{sgn}\,(\tau - t)\,\sigma T^4(t)E_2(|\tau - t|)\,dt \quad (16)$$

Back substituting Equation (15) and Equation (16) into Equation (9) gives us

$$\frac{1}{\tau^2}\frac{\partial}{\partial\tau}(\tau^2 q_R'') = 2\,E_2(\tau)\sigma T_\tau^4 + \frac{2}{\tau}\left\{2\sigma T_\infty^4 E_3(\tau) + 2\int_0^{\tau_o} \mathrm{sgn}(\tau - t)\sigma T^4(t)E_2(|\tau - t|)dt\right\}$$

$0 < \tau \le \tau_o$ (17)

3. GENRAL FORMULATION

The mixture in the cavity contains three components: the non-condensable gas Xenon, Uranium dioxide vapor, and fog. Initially there are only two components: Xenon and Uranium dioxide vapor at high temperature. But when the temperature of the mixture reaches the saturation temperature at time t= t_f, fog starts to form and moves to the colder regions at the bubble's wall as shown in (Fig. 3).
The conservation equations of the components (in molar units) can be represented as[18]:

$$\frac{\partial C_1}{\partial t} + \frac{1}{r^2}\frac{\partial}{\partial r}(r^2 N_{1r}) = r_1 \quad (18)$$

$$\frac{\partial C_2}{\partial t} + \frac{1}{r^2}\frac{\partial}{\partial r}(r^2 N_{2r}) = 0 \quad (19)$$

$$\frac{\partial C_3}{\partial t} + \frac{1}{r^2}\frac{\partial}{\partial r}(r^2 N_{3r}) = r_3 \quad (20)$$

Where r_1 the amount of UO_2 vapor per unit volume, and r_3 is the amount of fog per unit volume. When r_1 equals r_3, the condensed vapor is transferred from the hot region to the cold region at the same amount that is transformed to a fog [13].FromFick's first law of

diffusion, we can define $N_1 = x_1 Cv^* - CD\nabla x_1$, Where$N_1 + N_2 = Cv^*$, $c_i = \frac{\rho_i}{M_i}$, $x_i = \frac{C_i}{C}$ where $i = 1,2\ and\ 3$, $C = C_1 + C_2$[19].Chan, Cho and Condiff [56] assumed that the volume of the fog is insignificant and that it moves at the molar average velocity. Because the fog doesn't interfere with the diffusion components, such as UO_2 vapor and Xenon gas, the insignificant portion of the fog diffusion can be neglected, thus giving a near binary diffusion model.

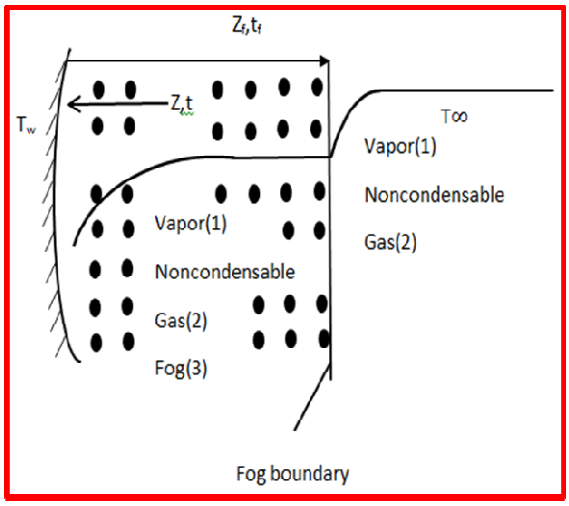

Figure 3. Fog boundary in two -phase mixture.

In this research the binary diffusion has been neglected between the UO_2 vapor and Xenon gas.According to this assumption the conservation Equations of the components (18), (19) and (20) becomes,

$$C\frac{\partial x_1}{\partial t} = -(1 - x_1)R(21)$$

$$C\frac{\partial x_2}{\partial t} = 0(22)$$

$$C\frac{\partial x_3}{\partial t} = (1 + x_3)R \qquad (23)$$

Now, the conservation equations of UO_2 vapor and fog can be solved together by eliminating R and solving for x_1 and x_3 as function of temperature. Note that the diffusion term is neglected in Equation (22) because it was assumed that the fog is moving with molar average velocity based on the Chan, Cho and Condiffsolution [13].Therefore, $C(1 + x_3) = C_0$, When $Z < Z_f$, $C_3 = 0$ and$C_1 + C_2 = C$,and C_0 is the initial value of the molar concentration and can be calculated from: $C_o = \frac{P_{UO_2}}{x_o RT_\infty}$, where P_{UO_2} is the UO_2 vapor pressure that can be calculated from[20, 13]:

$$P_{sat} = \frac{1}{10}\exp\left(69.979 - \frac{76800}{T_{sat}} - 4.34lnT_{sat}\right) \qquad (24)$$

In fog region$Z > Z_f$,the conservation Equations (21) and (23) may be solved together by eliminating R and applying the fog boundary condition$x_1 = x_{sat} and\ x_3 = 0$ gives us:

$\frac{1-x_1}{1+x_3} = 1 - x_{sat}$

(25)

Let$g_0(T) = \frac{P_v(T)}{C_o RT}$and from Equations (21, 23, and 25) together, a solution for x_1 ,x_3 can be obtained as [13],

$x_1(T) = \left[\frac{g_0(T)}{1-x_{sat}+g_0(T)}\right]$

(26)

$x_3(T) = \left[\frac{x_{sat}-g_0(T)}{1-x_{sat}+g_0(T)}\right]$

(27)

Upon using Equation (26) and (27) and solving for the local fog concentration C_3,

$C_3 = C_0[x_{sat} - g_0(T)]$

(28)

The total fog R produced can be computed by integrating Equation (28) from$\tau_f$to$\tau_o fog_{total} = \int_{R_i}^{R_o} C_3\, dV$as it indicated in Fig(4)[13].

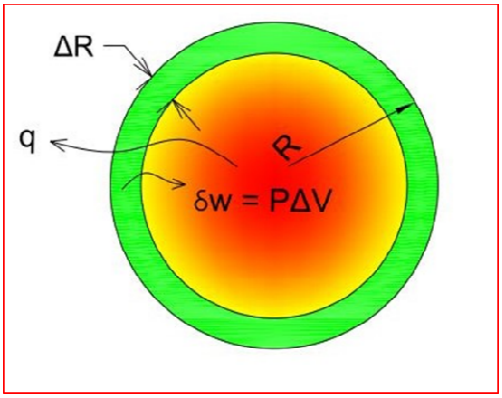

Figure 4. Fog thickness.

$m_{fog} = \frac{4\pi\, C_0 M_{UO_2}}{k^3} \int_{\tau_f}^{\tau_o} [x_{sat} - g_0(T)]\tau^2 d\tau$

(29)

Equation (29) gives us the amount of fog produced in grams.Where M_{UO_2} is the molecular weight of UO_2, and k is the absorption coefficientof UO_2.

4. HEAT TRANSFER MODELLING

To simulate fuel bubble's geometry as realistically as possible, according to experimental observation inFAST at ORNL, the energy equation must be reformulated into a spherical coordinate system. This equation was used with the radiative flux heat transfer equation (Equation 17) to obtain the effect of fuel bubble's geometry on the transient radiative heat flux. It was also used to predict the transient temperature distribution in the participating medium during a hypothetical core disruptive accident (HCDA) for liquid metal reactor (LMR) [21, 10].

$$(CC_p)\frac{\mathrm{DT}}{\mathrm{Dt}} = \frac{1}{\mathrm{r}^2}\frac{\partial}{\partial \mathrm{r}}\left(\mathrm{r}^2 \mathrm{k}\frac{\mathrm{dT}}{\mathrm{dr}}\right) + \mathrm{R}\,\mathrm{h_{fg}} + C\mathrm{D}\,\mathrm{r}^2\left(\mathrm{C_{p1}} - \mathrm{C_{p2}}\right)\frac{\partial \mathrm{x_1}}{\partial \mathrm{r}}.\frac{\partial \mathrm{T}}{\partial \mathrm{r}} - \frac{1}{r^2}\frac{\partial}{\partial \mathrm{r}}\left(\mathrm{r}^2 \mathrm{q}^{"}_{\mathrm{rad}}\right)$$

(30)

The total specific heat of the mixture can be calculated from, [18]$C_p = \sum_{i=1}^{3} x_i C_{pi}$

$$C_p = C_{p_2} + \frac{\left(C_{p_1} - C_{p_2}\right) g_0(T) + [x_{sat} - g_0(T)] C_{p_3}}{1 - x_{sat} + g_0(T)}$$

(31)

The body force and internal heat generation due to friction have been neglected during this derivation ofenergy equation, Moreover, the work done on the control volume due to friction is negligible because the flow is normal to the cavity – coolant interface. Equation (30) was simplified under these assumptions by assuming that the system is under local thermodynamic equilibrium, and the radiation dominates. Under these conditions, it was also assumed that the effects of other types of heat and mass transfer can be neglected such as convection, conduction and diffusion as compared with radiation heat transfer mode where it is radiating at high temperatures and high speed (comparable to the speed of light), but the other types of heat transfer are a relatively slow [13].In fog free region the energy equation can be reduced to:

$$(CC_p)\frac{\partial \mathrm{T}}{\partial \mathrm{t}} = -\frac{1}{r^2}\frac{\partial}{\partial \mathrm{r}}\left(r^2\, \mathrm{q}^{"}_{\mathrm{rad}}\right)$$

(32)

Upon substituting Equation (17) into Equation (32) gives us

$$-\frac{\partial \theta}{\partial t} = \frac{2k\sigma T_\infty^3}{CC_p}\left[\theta_\tau^4 E_2(\tau) + \frac{2}{\tau}\left\{\theta_w^4 E_3(\tau) + \int_0^{\tau_o} \mathrm{sgn}(\tau - t)\theta_\tau^4 E_2(|\tau - t|)dt\right\}\right]dt$$

$0 < \tau \leq \tau_o$(33)

$\mathrm{C} = 2\left\{\theta_w^4 E_3(\tau) + \int_0^{\tau_o} \mathrm{sgn}(\tau - t)\theta_\tau^4 E_2(|\tau - t|)dt\right\}$ and Let $\beta = \frac{2\,k\,\sigma\,T_\infty^3}{CC_p}$, back substituting into Equation (32) and integrating both sides from t = 0 to t = t gives usthe temperature distribution in fog free region,

$$\beta\, \mathrm{t}/(\tau) = \int_\theta^1 \frac{d\theta}{\left[\tau\, \theta_\tau^4 E_2(\tau) + C\right]} 0 < \tau \leq \tau_o$$(34)

The total heat flux in fog free region can be calculated from,

$$\tau^2 q_R'' = 2\,\sigma\, T_\infty^4 \int_0^{\tau_0}\left[\tau\theta_\tau^4 E_2(\tau) + C\right]\, \tau\, d\tau\, 0 < \tau \leq \tau_o$$(35)

Where θ(τ,t) is given by Equation (34).

In fog region, the transient temperature distribution profile and the wall heat flux can be extracted from the solution of the energy Equation (30) using the continuity Equations (21) and (23) for vapor and fog species respectively under the above assumption. This solution follows Chan, Cho and Condiff [56] procedures to reach the final form of the transient temperature distribution.

$$(CC_p)\frac{\partial T}{\partial t} + \frac{C}{(1 - x_1)} x_1' \frac{\partial T}{\partial t}\mathrm{h_{fg}} = -\frac{1}{\tau^2}\frac{\partial}{\partial \tau}\left(\tau^2 q_R^{''}\right)$$ (36)

By separating the variables and integrating from $\theta_{(f)} \rightarrow \theta$ and from $t_{(f)} \rightarrow t$ Equation (36) becomes,

$$\frac{\beta t}{\tau} = \int_{\theta_{sat}}^{1} \frac{d\theta}{[\tau_f \theta_{sat}^4 E_2(\tau_f) + C_{sat}]} + \int_{\theta}^{\theta_f} \frac{\eta(T)(1+\gamma(T))d\theta}{[\tau \theta_\tau^4 E_2(\tau) + C]} \; 0 < \tau \leq \tau_o \qquad (37)$$

Where $\beta = \frac{2\,k\,\sigma\,T_\infty^3}{C_\infty C_{p\infty}}, \eta(\theta) = \frac{CC_p}{C_\infty C_{p\infty}}$ and $\gamma(\theta) = \frac{h_{fg} x_1'}{C_p(1-x_1)}$

Equation (37) represents the transient temperature distribution in the fog region, and Trapezoid method techniques was used to compute the numerical integration.The wall heat flux at the bubble's wall can be obtained by the following relationship,

$$\frac{q_{rw(t)}}{2\sigma T_\infty^4} = \int_0^{\tau_f} (\tau\, \theta_\tau^4 E_2(\tau) + C)\, d\tau + \int_{\tau_f}^{\infty} [\tau\, \theta_\tau^4 E_2(\tau) + C] d\tau \quad (38)$$

Where $C = 2\{\theta_w^4 E_3(\tau) + \int_0^{\tau_o} \mathrm{sgn}(\tau - t)\theta_\tau^4 E_2(|\tau - t|)dt\}$Equation(38) consist of two regions. The first term on the right-hand side represents the wall heat flux in the fog free region, and the $\theta^4(t,\tau)$ is the transient temperature distribution vector in the fog free region. The second term represents the total heat flux in the fog region. Numerical integration was used to solve Equation (38) by using successive substitutions method.

5. The ABSORPTION COEFFICIENT IN RAYLEIGH MODEL

The absorption coefficient for small particle –size distribution can be calculated from [7]:

$$k_\lambda = -Im\{\frac{m^2-1}{m^2+2}\}\frac{6\pi f_v}{\lambda} \quad (39)$$

The complex refractive index of UO_2 is 2.42 - 0.009 i at λ = 600 µm [22], and the thermal wavelength of UO_2 was 0.4 µm [23]. The volume fraction f_v formula is defined as the ratio of resultant particle volume inside the bubble to the total bubble volume.The resultant particle volume of UO_2 = (m/ρ)/ (bubble volume).The amount of UO_2 was 1 gram in many of the CDV-argon tests [6], and for Rayleigh scattering model the geometric mean diameter dg was selected as 0.015 µm based on the particle size distribution in reference [6]. The liquid density of UO_2 is 8125.7 Kg/m [24].

6. RESULTS AND DISCUSSION

These analyses are applied to estimate the bubble collapse time and to study the safety profile of LMR reactors during hypothetical core disruptive accident (HCDA). In Rayleigh model (non-scattering model) with fog formation problem are investigated in the present paper by using spherical bubble geometry. In this model the particle size of UO_2 was observed in FAST at ORNL to be in range 0.1 µm [6], and the absorption coefficient was estimated from Equation (39) which is equal to (k = 10 m^{-1}). The latent heat of condensation of UO_2 vapor was calculated from $h_{fg} = 516382 - 22.946TJ$ mol^{-1} [25], and the specific heats at constant pressure of UO_2 vapor, Xenon, and liquid condensate are 20.02, 12.55 and 135.56 J/mol K [13]. The vapor pressure of UO_2 vapor is 0.2655 MPa which gives T_{sat} = 4000 K and the total pressure is 0.3 MPa [13]. The

super heat temperature and the coolant temperature are 4050 K and 811 K respectively [9, 13].The Figures (3-4), (3-5), and (3-6) show the temperature distributions in fog region and fog free at R = 0.1 m and t = 1.85 ms, R = 0.1 m and t = 2.5 ms, R = 0.1 and t = 3.5 ms. These figures show the fog penetration depth values at t = 5 ms equals to τ_f = 0.32 and t = 2.5 ms equals to τ_f= 0.42 .It's clear from these results that the fog penetration depth is increases as the time increases and it's values smaller than one (i. e. $\tau < 1$) or in other words the medium is an optically thin medium.

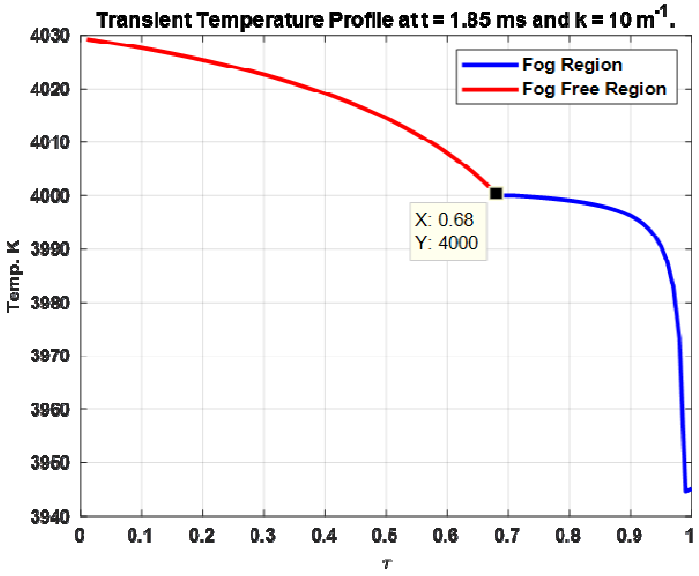

Figure 5. Transient temperature profile in spherical coordinates at t = 0.9 ms.

As the bubble cools down the wall temperature drops and the optical thickness increases as indicated in Figures (5, 6, and 7). The important conclusion that can be drawn from Figures (5, 6, and 7) is the presence of fog resulting from adiabatic expansion of Uranium dioxide and Xenon gas enhances the temperature distributions in fog region.

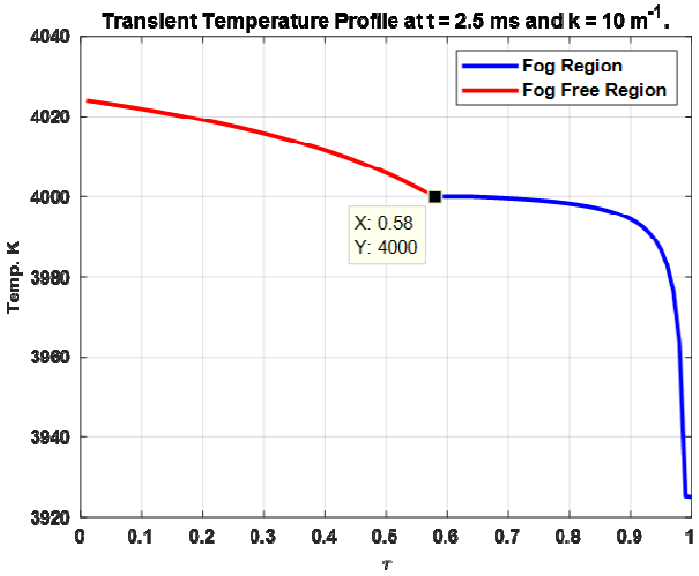

Figure 6. Transient temperature profile in spherical coordinates at t = 5 ms

The non-condensable gas will inhibit condensation in either heterogeneous or homogenous (fog formation) by dew point suppression, and the presence of Xenon gas has the effect of lowering the saturation temperature of the UO_2 vapor (Dew Point Suppression) in the mixture.The presence of non-condensable Xenon gas in the mixture delays the condensation process, and the time delay in this process is dependent on its concentration level in the mixture.

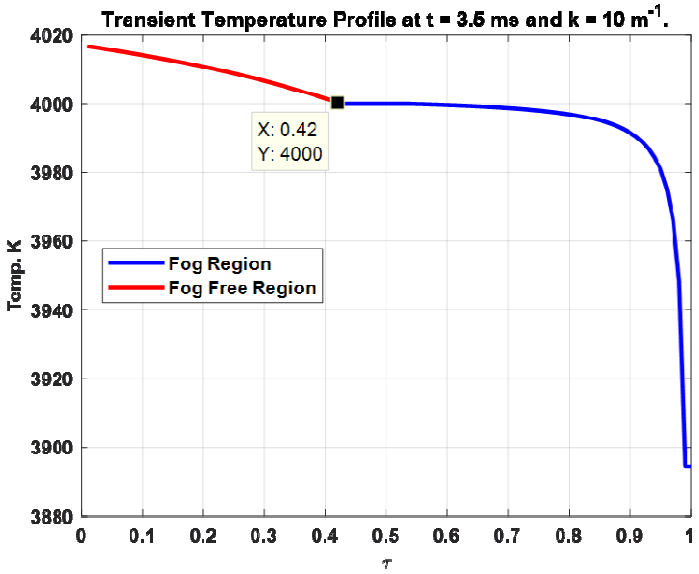

Figure 7.Transient temperature profile in spherical coordinates at t = 10 ms.

In comparison between Figure (5) and Figure (7) the wall temperature was decreasing from 3945 K to 3888 K at R = 0.1 m. The reduction of wall temperature is valuable conclusion where is no Sodium vaporization will occur at the bubble surface. This reduction in wall temperature was due to absorption effects inside the bubble which is higher in small bubbles. Moreover, no collapse will occur in the stainless-steel vessel of the reactor because the bubble is cools down rapidly due to the coolant heat sink effect. In the fog region the latent heat of condensation sustains the temperature distribution profiles and keeps it at high levels and drops suddenly at the bubble's surface due to heat loss by radiation through the sodium coolant which has high thermal conductivity and low emissivity [26].The absorption coefficient increases the loss of radiation due to absorption will increase, and the attenuation of the thermal radiation inside the participating medium will occur toward the bubble's wall. In other words, more energy destroyed by the medium. The effect of the absorption coefficient on bubble collapse time was resulting from the e-folding length (r*) effect which can be defined as, the distance at which the intensity (I) drops to 38 % from its initial value. For pure absorption $\frac{I}{I_0} = e^{-kr^*}$, so when k=10 m^{-1} the e-folding length r*=10 cm.Figure (3-6) shows the transient heat flux in spherical coordinate's system vs time near to the bubble's wall at R = 0.1m and k = 10 m^{-1}. This curve represents the values of transient heat flux with fog formation. Figure (9) shows the presence of fog resulting from the adiabatic expansion of Uranium dioxide and Xenon gas will enhance the radiative heat flux at the boundary because the latent heat of condensation sustains the temperature of the fog and keeps it near to the saturation temperature.Figure (9) shows that as the volume of bubble increases, the wall heat flux increases because of the thermal absorption effect

inside the bubble, which is higher in small bubbles compared with large bubbles that contains the same amount of mass (of UO_2 particles). In small bubbles more energy is absorbed or destroyed by medium because the medium is optically dense compared with large bubbles.

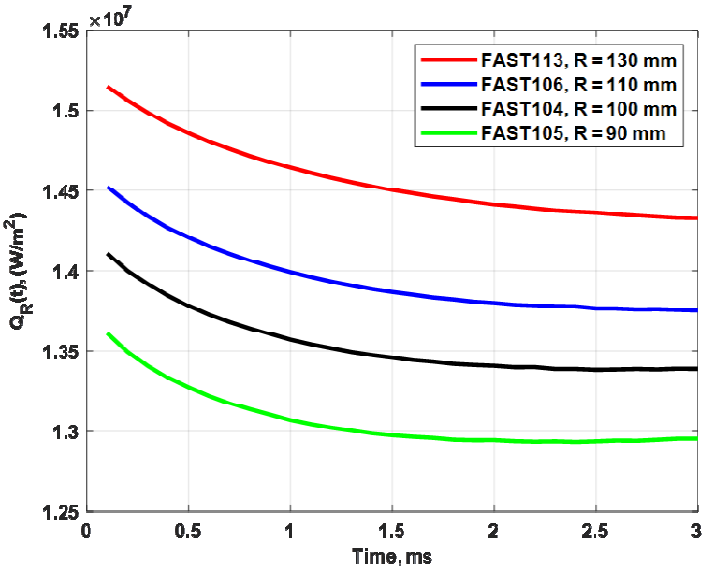

Figure 8.Transient heat flux at wall for sphere at R = 0.1 m.

7. APPLICATION OF THE THEORY

This assessment is based on a comparison of the bubble rise time, computed using the Taylor formula, against the elapsed time required for energy transfer by radiation out of the bubble [10].

$$t = \frac{H}{\sqrt{g\,R}} \quad (40)$$

Where H is the vertical distance above the bubble.R is the bubble radius.g, is the acceleration of gravity in SI units 9.81 m/s^2. Equation (29) was used to compute the condensation time of UO_2 vapor (bubble collapse time) Based on the temperature distribution in fog region that as indicated on Figure (5), Figure (6) and Figure (7). Referring to these Figures the wall temperature and the saturated temperature are varying from T_{wall} to T_{sat} in sodium experiments, and the maximum radius is listed in [23, 10] under Sodium data. Using the Math Lab application, the trapz function is used to estimate the integral of Fog Production Equation (29) to compute the amount of condensed UO_2 vapor (fog). Based on these calculations that were done on the capacitor discharge vaporization (CDV) experiments conducted in FAST Facility at Oak Ridge Laboratory, the bubble's collapse time is smaller than the bubble's rising time as it obtained in Table 1. Figure 9 was designed at 1-gram mass of UO_2 vapor transformed to fog. It shows that large the bubble collapses faster than the small bubbles, because it has lower volume fraction ratio (resultant particle volume/ bubble volume). In other words, the radiant

energy destroyed by the participating medium inside the large bubble is smaller than the small bubbles. At the same time the large bubbles its temperature distribution is higher than the small bubbles, because low radiation losses occurred inside it.

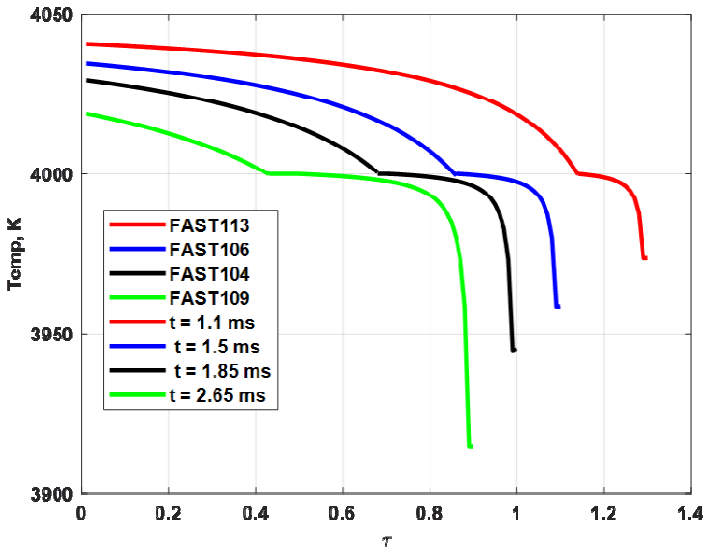

Figure 9. Transient temperature profile and fog penetration depth.

This means that there is no aerosol release from the FAST vessel to the cover gas because all the UO_2 particles will condense before the bubble reaches the cover-gas or breaking the surface and releasing bubble contents [5].

Table 1. Comparison between bubble collapse time and bubble rise time.

Expert. #	Calculated Aerosol Mass m_{fog} (g)	External Radius R_{Edge} (m)	Collapse Time (mS)	Rise Time (S)[63]
FAST104	1	0.1	15.5 ms	1.07 s
FAST106	1	0.11	10.4 ms	0.23 s
FAST107	1	0.1	15.5 ms	0.14 s
FAST108	1	0.08	6.8 ms	0.0903 s
FAST109	1	0.09	15.7 ms	0.11 s

FAST113	1	0.13	8 ms	0.026 s

This means that there is no aerosol release from the FAST vessel to the cover gas because all the UO_2 particles will condense before the bubble reaches the cover-gas or breaking the surface and releasing bubble contents [5].

8. CONCLUSIONS

This assessment In Rayleigh model, the radiatively managed fog formation in high temperature condensable mixture has been investigated, in spherical bubble that has small size UO_2 particles. The amount of aerosol release from the bubble to the covergas can be predicted from Equation (29), which is a new important contribution to HCDA. In addition, the effect of the fuel bubble's geometry on the radiative heat flux and the transient temperature distribution in the participating medium during a hypothetical core disruptive accident (HCDA) for a liquid metal cooled reactor (LMR) has been investigated. Finally, based on the experimental data conducted in the 1980's at the Fuel Aerosol Simulant Test (FAST) facility at Oak Ridge National Laboratory and the results have been tabulated in Table (1) regarding the bubble rising time and the bubble collapse time. The conclusion that can be drawn from the data is that the Fuel Aerosol Simulant Test (FAST) facility at Oak Ridge National Laboratory has a larger margin of safety since the bubble rising time is greater than the bubble collapse time.

NOMENCLATURE

upper case

B, surface radiosity, ($W/m^2/m$)

C, molar concentration, (mol/m^3)

C_p, molar specific heat at constant pressure, (J/mol K)

D, diffusion coefficient (m^2/s)

E_i, exponential integral of ith kind (dimensionless)

H, pool level relative to the vaporizer, (m)

I, Radiation intensity, (W/m^2sr)

M, molar weight (g/mol)

N, molar flux (mol/m^2 s)

P, pressure, (Pa)

R, bubble radius, (m)

R, molar fog production rate/volume, (mol/m^3 s)

R_i, R_o, internal and external radius, (m)

T, temperature, (K)

T_i, initial temperature level of coolant, (K)

V, volume, (m^3)

X, The molar fraction, (dimensionless)

Z, physical coordinate normal to the wall, (m)

lower case

c_p, constant pressure specific heat, (J/kg K)

$e_{b\lambda}$, spectral black body emissive power ($W/m^2/m$)

g, gravitational acceleration, (m/s^2)

h_{fg}, the latent heat of condensation, (J/mol K)

k, thermal conductivity, (W/m-K)

m, the mass, (g)

n, the index of refraction, (dimension less)

$p(\mu, \mu')$, The scattering phase function, (dimension less)

$q''_{R\lambda}(\tau_\lambda)$, The monochromatic radiation flux, (W/m^2)

v^* , Molar average velocity, (m)

t, time, (s)

q_r, radiative flux (W/m^2)

r_i, molar fog production rate/volume, (mol/m3 s)

z, bubble displacement, (m)

Greek

β, function, (s^{-1})

β_λ, Spectral extinction coefficient, (m^{-1})

γ, function, (dimensionless)

δ, e-folding length, (m) [Distance over which the exponential function diminishes by a multiplicative factor of 0.3678… i.e., e^{-1}.]

ε, coolant emissivity (dimensionless)

η, function (dimensionless)

ρ, density, (kg/m^3)

t, time, (s)

θ, polar angle, (rad)

μ, the cosine direction of θ (rad)

τ_λ , optical coordinate, (dimensionless)

φ, Azimuthal angle, (rad)

σ_λ, Spectral scattering coefficient, (m^{-1})

σ, Stefan Boltzmann

ω_λ, Albedo of scattering, (dimensionless)

subscripts

c, a condensation heat transfer quantity

max, maximum value

sat, saturation property

r, a radiation heat transfer quantity

R, quantity evaluated at r = R

B, bubble related quantity
∞, far-field quantity

w, wall

sat, saturation

λ, wavelength, (m)

τ, varying with τ- direction

REFERENCES

1. A. Brunett, R. Denning, M. Umbrel, W. Wutzler, "Severe Accident Source Terms for a Sodium-cooled Fast Reactor", *Annals of Nuclear Energy*, **64 ,**pp. 220-229 (2014).
2. F. J. Arias, G. T. Parks, "An Estimate of the Order of Magnitude of the Explosion during a Core Meltdown-Compaction Accident for Heavy Liquid Metal Fast Reactors: A Disquieting Result Updating the Bethe-Tait Model", *Progress in Nuclear Energy*, **79**, pp. 182-189, (2015).
3. D. A. Powers, B. Clement, R. Denning, S. Ohno, R. Zeyen, *Advanced Sodium Fast Reactor Source Terms: Research Needs*, SAND2010-5506, Sandia National Laboratory, (2010).
4. A. Minato, N. Ueda, D. Wade, E. Greenspan, N. Brown, *Small Liquid Metal Cooled Reactor Safety Study*, UCRL-TR-217093, Lawrence Livermore National Laboratory, (2005).
5. J. C. Petrykowski, "The Energtics of Coolant-Bubble-Covergas Interactions Associated with LMR out-of-Reactor Source Term Experiment," in NURETH-16, Chicago, 2015.
6. K. Chen, "Particle-Size Distrubution in Capacitor Discharge Vaporization of Uranium Dioxide," Nuclear Science and Engineering, pp. 459-472, 1982.
7. Modest, Radiative Heat Transfer, Hightstown: McGraw-Hill,Inc, 1993.
8. A. B. Reynolds, "The UVABUBL Program and its Application to the fast-underwater Test," Nuclear Engineering, pp. 199-222, 1987.
9. J. C. Pertykowski, "Analysis of Fuel-Coolant Interaction Potential in Sodium Cooled Fast Reactor Safety Experiments.," in ICONE20, Anaheim, Califorina, 2012.
10. M. L. Tobias, "Analysis of the Heat and Mass Transfer Processes of a UO2 Bubble in Sodium.," Proceedings of the International Meeting on FAST Reactor Safety

TECHNOLOGY, Seattle, 1979.
11. M. L. Tobias, "Analysis of the Heat and Mass Transfer Proccesses of a UO2 Bubble in Sodium for the Fuel Aerosol Simulant Test.," in NUREG/CR-0678;ORNL/NUREG/TM-307, Tennessee, 1979.
12. M. L. Corradini, "Heat Transfer and Fluid Flow Aspects of Fuel - Coolant Interactions.," Massachusetts Institute of Engineering, Cambridge, Massachusetts, 1978.M. L.
13. S. H. Chan, "Heat Transfer from a High Temperture Condensable Mixture," Int. J. Heat Mass Transfer, pp. 63-71, 1979.
14. S. G. Taylor, "The Mechanics of Large Bubbles Rising through Extended Liquids and throughLiquids in Tubes," The Royal Society Publishing, pp. 375-390, 1949.
15. M. N. Ozisik, Radiative Transfer, New York : Wiley , 1973.
16. J. R. Howell, Thermal Radiation Heat Transfer, New York: CRC Press, 2011.
17. E. M. Sparrow, Radiation Heat Transfer, Belmont, California:HemispherePublishing Corporation, 1978.
18. Bird, Transport Phenomena, New York:Wiley&Sons, 2001.
19. Incropera, Fundamentals of Heat and Mass Transfer, New York : Wiley , 1996.
20. M. L. Corradini, "The Effects of Sodium Entraintment and Heat Transfer with Two-Phase UO2 during a Hypathetical Core Disruptive Accident," Nuclear Science and Engingeering, pp. 242-258, 1979.
21. Kays, Convection Heat and Mass Transfer, New Delhi: Tata McGraw Hill , 2005.
22. Atsuyuki Suzuki, "Noval Technique for Manipulating Mox Fuel Particles Using Radiation Pressure of A Laser Light.," in International Youth Nuclear Congress, Tokyo, 2000.
23. J. C. Petrykowski, "Aerosol Release Experiments in The Fuel Aerosol Simulant Test Facility: under Sodium Experiments," ORNL/TM-9479,Oak Ridge National Laboratory, Oak Ridge, Tennessee, 1985.
24. Iosilevski, "Equation of State of UO2," International Journal ofThermophysics , vol. 22, no. 4, pp. 1253-1264, 2001.
25. J. K. Fink, "Thermophysical Properties of Uranium Dioxide," Journal of Nuclear Materials, pp. 279,1-18, 1999.
26. R. L. Webb, "Analysis of Fast under Sodium Tests," in ANS/ENS Fast Reactor Safty, TN, 1985.

